RESEARCH PAPER

Determination of shale types and their volumes and petrophysical exponents for more accurate water saturation estimation for Raha Formation, Gulf of Suez, Egypt

Tarek F. Shazly [a], Ahmed Z. Nouh [a], Marwa Z. El-Sawy [a,*], Mazen El-Bay [b]

[a] Egyptian Petroleum Research Institute, 11727 Nasr City, Cairo, Egypt
[b] Services Gmbh Middle East, Cairo, Egypt

Abstract

This study depends on the analysis of well logging data for the Raha Formation, utilizing eight wells scattered in the Ras Budran Oil Field. It is situated in the northern region of the Gulf of Suez's Belayim Offshore Oil Field and is 4 km away from the Sinai coast. Water saturation is one of the steps through which the characterization of the reservoir and prediction of future accumulation are determined. Many parameters, such as types of shale, volumes of each type, and petrophysical exponents, are necessary to detect the accurate estimation of water saturation. First, Dia-Porosity crossplots are used to estimate three types of shale and their volumes (dispersed, laminated, and structural). From these plots, it was found that the dispersed shale exhibits the highest percentage in the middle of the study area, while the laminated shale volume increases toward the north directions, but the structural shales give the maximum value in the north-west trend. The presence of scattered shale in a formation is known to have a negative impact on the permeability of the rock, unlike the laminated shale, which decreases the total average of effective porosity. Comparable to laminated shale, structural shale has nearly identical characteristics. Second, the petrophysical exponents (cementation factor (*m*), saturation exponent (*n*), and tortuosity factor (*a*) were ascertained using Pickett's plot. It gave the values of *m* ranging from 1.8 to 2.3 and values of *a* varying from 0.72 to 1 in the studied wells, where these petrophysical exponents play a vital role for calculating the water saturation (Sw) in both clean and shaly rocks. This study aimed to determine the different types of shale and calculate the petrophysical exponents, which are important for a good estimation of the water saturation in rocks (clean and/or shaly) and for determining hydrocarbon saturation (Sh).

Keywords: Petrophysical exponents, Petrophysical parameters, Pickett's plots, Ras budran oil field, Shale types

1. Introduction

The reservoir characterization is an essential target for the estimation of the future vision of reservoir evaluation. There are many numbers of errors that interfere with the calculations related to the prediction of reservoir evaluation; with these errors, no precise and suitable reservoir properties, which leads to the loss of essential values for reserve contents and then hydrocarbon production.[1]

Determination of the true percentage of water saturation is considered one of the most important difficulties associated with the determination of accurate petrophysical parameters. The difference in the calculated water saturation may lead to considerable differences in the estimated oil saturation, types of shale, volume of each type, and petrophysical exponents are very important items that affect the accurate evaluation of water saturation and then accurate estimation of oil saturation.

Received 9 November 2023; revised 2 December 2023; accepted 7 December 2023.
Available online 8 April 2024

* Corresponding author at: Egyptian Petroleum Research Institute, Egypt.
E-mail address: Marwa_epri@yahoo.com (M.Z. El-Sawy).

https://doi.org/10.62593/2090-2468.1002

The present work is applied on eight digitized wells (RB-A2A, RB- AI, RB-B3, RB-B1, RB-C1A, RB-B8B, EE85-2, and RB-C2) for Raha Formation. These wells were dispersed around the northern portion of the Belayim offshore area in the Ras Budran Oil Field. Where, this area has latitudes between 28°57′ and 28°59′ N; and longitudes lies between 33° 7′ and 33° 9′ E, Gulf of Suez (Fig. 1).

Due to the economic potential and geological history, the Gulf of Suez region was differentiated by its geological features. In some places, there are a number of structural characteristics that contributed to the inferred rift tectonics and caused the Red Sea and the Gulf of Suez to form.

The shale volume is important in determining the shale content percentage depending on the eight accessible wells. Also, the type of shale and volume of each type was determined by the application of the Dia-Porosity crossplots which is very effective and helpful in determining the shale types and their volumes (dispersed, laminated, and structural). These plots exhibited that the dominant shale type is the dispersed shale.

Pickett's plots are utilized to determine different types of petrophysical exponents (*m*, *n*, and a) necessary for determining water saturation accurately; where these parameters are included in the equations of water saturation, where it is not accurate to put these parameters as constants.

2. Geological setting and stratigraphy

Situated in the northern region of the Belayim offshore field, the Ras Budran Oil field is ~4 km away from the eastern side of the Gulf of Suez. It has latitudes 28°57° and 28°59° N, and longitudes 33°7° and 33°9° E as its boundaries (Fig. 1). Based on the seismic interpretation deduced at the base of Miocene evaporates in 1987,[2] Ras Budran Oil Field was discovered after drilling EE85-1 well which penetrated a length of about 1500 ft of sandstone oil reservoir of Raha and Nubian Formations with age range from Cenomanian to Paleozoic. The geology background of the Gulf of Suez has been extensively discussed in many earlier studies, particularly in the study area.[3,4]

Ras Budran Oil Field has been developed from three well-head platforms with 18 development and water injector wells. The targeted rock unit was penetrated by drilling eight horizontal wells scattered throughout the Raha Formation. The studied wells are RB-A1, EE85-2, RB-B8B, RB-B1, RB-C2, RB-C1A, RB-B3, and RB-A2A is shown in Fig. 1. The age of the entire rock sequence ranges from Pre-Cambrian to recent,[5] it was penetrated as shown in Fig. 2.

Ras Budran Oil Field takes the crest of a platform that has a trend in the NE–SW direction. It is perpendicular to the Gulf of Suez's primary trend. Many previous research studies indicated that the structures were divided into several parallel plates through a group of clysmic faults taking the

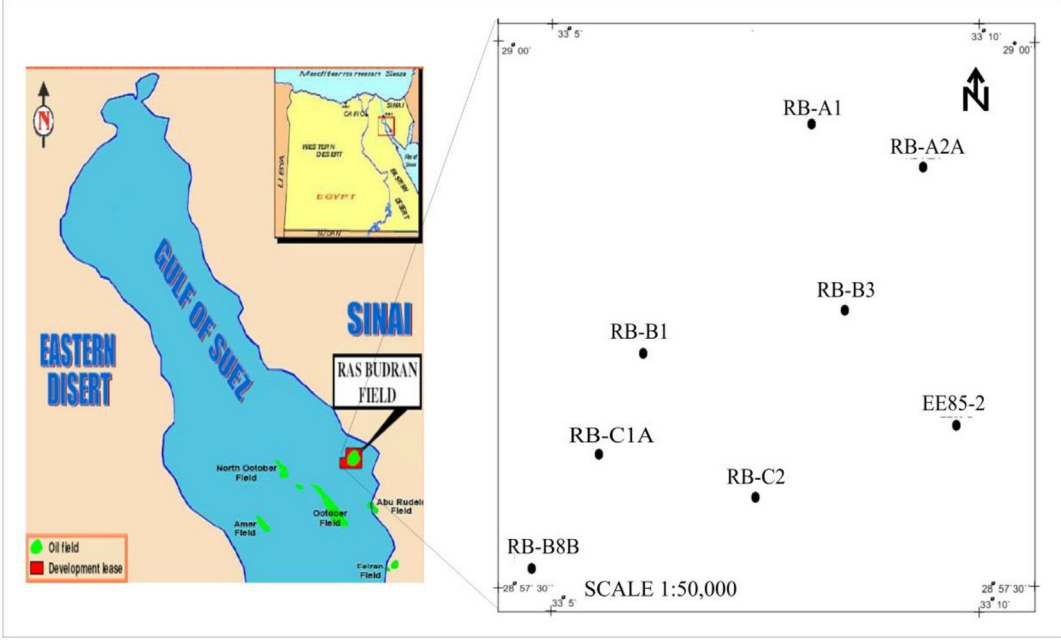

Fig. 1. Location map and distribution wells of Ras Budran Oil Field.

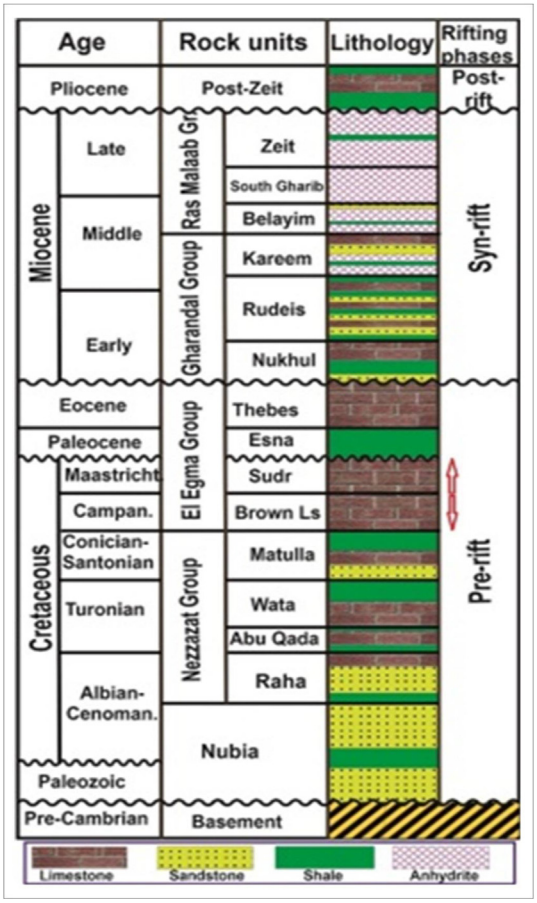

Fig. 2. General lithostratigraphic chart of Ras Budran Field, Gulf of Suez (modified after[5]).

direction of NW–SE.[6] Numerous structural and stratigraphic investigations were carried out in the subject region.[7–9]

Depending on lithological, palynological, well logging, analysis well, and production evaluation of Nubian and Lower Raha sandstone, the reservoir section has been classified into five reservoir units. These units were remarked as U I, U IIA, U IIB, U III, and Lower Raha.[10] Boundaries of these sedimentary reservoir units are conformable except, for a regional unconformity between U I of the Paleozoic age and U IIA of early Cretaceous age.

These reservoir units are discussed from bottom to top as follows:

(1) Reservoir Unit-I:

This rock unit consists of nonfossil fereous fine to medium-grained sandstone, kaolinitic intercalation. It is represented by the Nubia 'C' and 'D' series of the Paleozoic age.

(2) Reservoir Unit II-A:

This rock unit is represented by nonfossil fereous medium to coarse-grained sandstone, kaolinitic at parts, siltstone, and red shale intercalations of the early Cretaceous age. This rock unit unconformable overlies U I with the age of Paleozoic. The eroded surface nature of UI leads to its thickness variation from one well to another.

(3) Reservoir Unit II-B:

It mainly consists of medium to coarse-grained sandstone and thin shale streaks with an early age of Cretaceous. The same depositional regime leads to the same variation of thickness.

(4) Reservoir Unit-III:

The main composition of this rock type is sand and sandstone with some interbeds of shale related to the early Cenomanian age, which conformably overlies U IIB of the early Cretaceous age.

(5) Reservoir Unit Lower Raha:

The formation studied in this work mainly consists of sandstone with a few beds of shale scattered in the formation, which is related to the age of early Cenomanian. The maximum and minimum thickness is observed in B6 and A3B well of about 287 and 179 ft, respectively. In addition to the above five reservoir rock units, there are many reservoirs in Middle and Upper Raha rock types which mainly consist of sandstone, shale, and some rocks of limestone from the age of late Cenomanian. The two rock units underlies the Abu Qada Formation of the Turonian age.

Ras Budran Oil Field is studied as a solitary structure feature, where this field is trending to the direction of northeast–southwest (Fig. 3).

Ras Budran Oil Field has a structure that is interpreted as northeast dipping fault blocks. These fault blocks are constructed from a system of antithetic faults down stepping to the southeast and are finally bounded to the south and the west by major faults having a cumulative throw around 2000 ft while to the north and east, the structure is surrounded by a major synthetic faults.

3. Methodology

At first, an isopach map was drawn to show the variation in thickness in the studied area. It is known that the presence of shale content in any formation has a negative effect on determining the total porosity, effective porosity, and permeability and thus the amount of liquid present in the formation.[11] One of the most important effects of shale present in

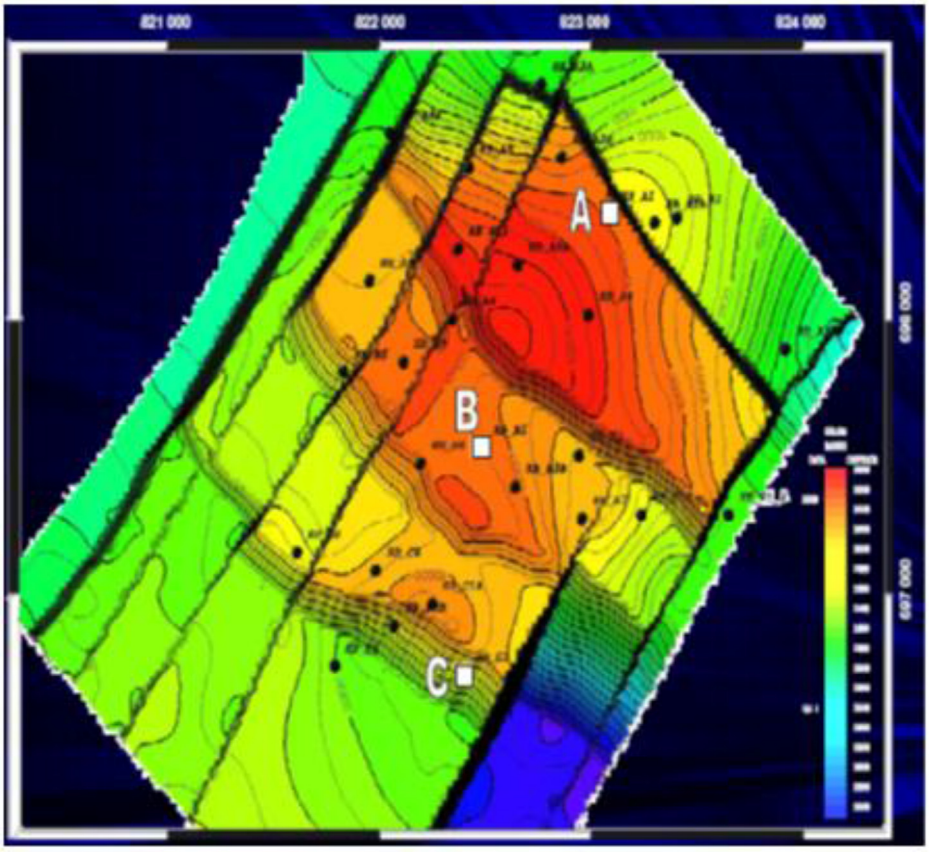

Fig. 3. Structure contour map of Ras Budran Oil Field.

the formation is to decrease the resistivity contrast between oil, water, and gas[12] then, shale content is an important quantitative factor of log analysis. In other words, the shale volume is needed to correct the porosity value and water saturation resulting from the partial effect of shale volume. The presence is considered one of the most important indicators that express the quality of the reservoir. The less its presence, the higher the quality of the reservoir, which is considered the better reservoir. In the present work Dia-Porosit crossplots will be utilized to determine the different types of shale that help in choosing the suitable shale model. Also, the petrophysical exponents (*m*, *n*, and *a*) are required for the corrected values of water saturation. To achieve this purpose, Pickett's plot was used for calculating the different petrophysical parameters for applying them in Archie's equation.[13]

4. Results and discussions

4.1. Shale volume determination

The following technique was applied in this paper to determine the volume of shale. The proportion of the gamma-ray index can be found using the following formula (IGR).[14]

$$\mathrm{IGR} = \frac{\mathrm{GR_{log}} - \mathrm{GR_{min}}}{\mathrm{GR_{max}} - \mathrm{GR_{min}}} \quad (1)$$

Where IGR is identified as the value of gamma-ray index, $\mathrm{GR_{log}}$ is the value of gamma-ray reading for each zone, $\mathrm{GR_{min}}$ and $\mathrm{GR_{max}}$ are the values of minimum and maximum gamma rays.

Then, the volume of shale percentage can be calculated by using the values of gamma ray index, by using the following equation.[15–17]

$$\mathrm{Vsh} = 0.33\,[22 * \mathrm{IGR} - 1.0] = \mathrm{x} \quad (2)$$

4.2. Estimation of the shale types and their volumes

There is a relationship between the rock resistivity and the water saturation. This relationship is calculated using the Archie water saturation equation but in the presence of water that contains only electrically conductive material within the formation. However, in the case of the presence of other conductive materials, such as shale rocks, the Archi

equation must be modulated to suit the conductive materials present. To connect the rock resistivity to water saturation in the shaly formation, a new model needs to be created.[18]

The concept of rock porosity is further complicated by the presence of shale, thus it affects the quality of reservoir. This porosity, however, does not serve as a prospective hydrocarbon reservoir. Therefore, as a prospective hydrocarbon resource, high total porosity but low effective porosity may be present in the shale of the shaly formation. As a potential hydrocarbon reservoir, its porosity is not accessible. shale of the shaly formation, for instance, may have a high total porosity but a low effective porosity, making it a possible hydrocarbon resource.

The proportion of shale present, the shale's physical features, and the change in the percentage of minerals present in it have a role in the reading of the percentage of gamma rays up and down throughout the length of the well.

Shale distribution within the formation also depends on this. The distribution of shaly components in the formation can be done in three different ways, it was discovered as the following.

4.2.1. Laminated shale

In between sand layers, shale can appear as laminae. Not the porosity or permeability of the sand streaks themselves is affected by laminar shale. However, the average effective porosity decreases proportionally when the amount of laminar shale is raised, and the overall amount of porous medium is correspondingly reduced.

4.2.2. Structural shale

In the matrix of formation, shale can be found as nodules or grains. This matrix shale is referred to as structural shale, and it is typically thought to have features similar to laminar shale and nearby massive shales.

4.2.3. Dispersed shale

By partially filling the intergranular spaces, the shaly material can be dispersed as dispersed shale throughout the sand. The shale that has been distributed may be found in groups that adhere to or cover the sand grains, or it may fill the tiny pore channels. The total permeability of the deposit is significantly reduced by dispersed shale in the pores.

4.3. Theory of the technique

One of the most critical and precise graphical logging methods used to analyze the petrophysical parameters is the Dia-Porosity crossplot. Various porosity tool combinations, including density (D), neutron (N), and sonic (S), are dependent on these plots. According to Schlumberger,[19] this is done to identify the types of shale, which may be laminar, dispersed, or structural, as well as the effective porosity (e), which plays a significant impact on the productivity of hydrocarbons.

The total volume of dispersed shale is abbreviated as VD, the total volume of laminated shale is abbreviated VL, and the total volume of structured shale is abbreviated VS.

Dia-Porosity crossplots for the investigated wells are shown in Fig. 4 for RB-A1 well, as an example. The points (Q), (S_d), and (Sh_o) represent the quartz point, the clean point, and then the shale point, respectively.[19]

The sand line is a line connecting between Q (0,0) and S_d (ϕ_{Nsd} and ϕ_{Dsd}) points and is expressed as:

$$\phi D = \phi N \tag{3}$$

Also, the shale line is a line connecting between Q (0,0) and Sh_o (ϕ_{Dsh} and ϕ_{Nsh}) points and is expressed as:

$$\phi D = (\phi Dsh \ / \ \phi Nsh)\, \phi N \tag{4}$$

The lines of constant porosity in the crossplot are perpendicular to the shale line (Q-Sho). The range of their porosities is from zero on the shale line to maximum porosity on the line through point S_d. The equation for the constant porosity lines is as follows:

$$\phi D = (\phi Dsh \ / \phi Nsh)\phi N + (1 - \phi Dsh \ / \ \phi Nsh)\, \phi N \tag{5}$$

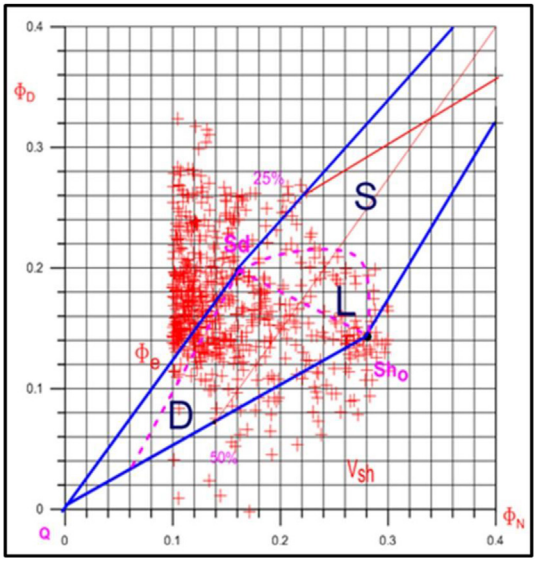

Fig. 4. Dia-Porosity crossplot of Raha Formation in RB-A1 well in the studied area.

Parallel to the clean sand line (Q-Sd) is the volume of shale (vsh) constant lines. On the clear sand line, they range from Vsh = 0 to Vsh = 100% at the Sho point. The following equation represents the constant shale lines:

$$\phi D = \phi N + Vsh\,(\phi Dsh - \phi Nsh) \quad (6)$$

By solving the two equations for ϕ and V_{sh} for water-bearing formations it will give:

$$\phi = [\phi D - (\phi Dsh / \phi Nsh)\,\phi N]/1 - (\phi Dsh / \phi Nsh) \quad (7)$$

$$Vsh = (\phi D - \phi N) / (\phi Dsh - \phi Nsh) \quad (8)$$

Laminated shale's points will lie on the Sd-Sho line, whereas dispersed shale's points will veer to the left of the line, and the structural shale's points will veer to the right side.

As indicated by equations (9)–(13), the volumes of the three different types of shale can be determined.

The plotted point (P_1) in the crossplot has the values of ϕ_1 and V_{sh1}, which can be calculated through the following equation:

$$Vsh1 = VD + VL + Vs \quad (9)$$

From P1 to P2, point P1 is moved along line D until it intersects the S + L envelopes. Because the remaining shales are laminated and structural, VD = 0, hence the values of ϕ_2 and V_{sh2} can be found at P2, where:

$$Vsh2 = VS + VL \quad (10)$$

Passing through P2 and a line of constant porosity, the second displacement is carried out. This line crosses the laminated shale line at point P3, which can be used to calculate the values of porosity and Vsh3 after passing through P2 where:

$$Vsh3 = VL \quad (11)$$

The structural shale volume can be defined using the prior equations as follows:

$$Vs = (VS + VL) - VL$$

$$= Vsh2 - Vsh3 \quad (12)$$

Additionally, the following equation can be used to estimate the volume of dispersed shale:

$$VD = Vsh1 - Vsh2 \quad (13)$$

4.4. Lateral distribution maps of Raha Formation

4.4.1. Isopach map

The contour lines on the isopach map are drawn through points of various thicknesses, where the equal points of the values are contoured together in the stratigraphic unit under study. Fig. 5 shows an isopach map of the studied area where it shows variation thicknesses in Raha Formation between eight wells in the study rock formation. The horizontal thickness of the rock unit increases in the north direction, where the maximum value is shown in RB-A1 and RB-A2A wells (550–488 m, respectively) while the rock unit decreases in the middle and the south direction. The minimum value is recorded at RB-B3 and RB-C2 wells (20–70 m, respectively).

4.4.2. Shale volume distribution map of Raha Formation

From the values of shale volumes, the horizontal distribution map was established, which shows that the shale's maximum value is shown by the RB-C2 and RB-B3 wells in the center of the map (Fig. 6), the maximum values of these wells are 0.288 and 0.28, respectively. This map shows a gradual decrease toward the NE and SW directions.

4.4.3. Dispersed shale distribution map of Raha Formation

A distribution map of dispersed shale is shown in Fig. 7. This map shows the presence of general relatively low in N–W, N-E, and S-E directions of the map. It gradually increases to the middle part,

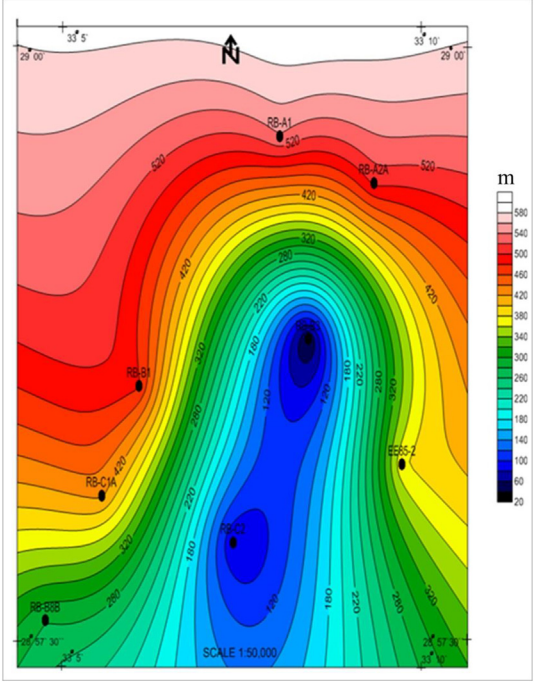

Fig. 5. Isopach map of Raha Formation in Ras Budran Oil Field in the studied area.

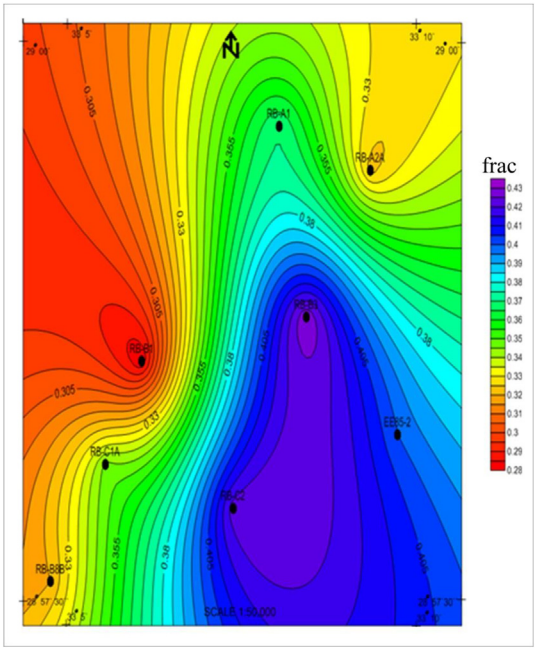

Fig. 6. Shale distribution map of Raha Formation in the studied area.

where the maximum percentage (0.152) is recorded in the RB-B3 well.

4.4.4. Laminated shale distribution map of Raha Formation

The laminated shale distribution map was exhibited in Fig. 8. It reveals a general north east

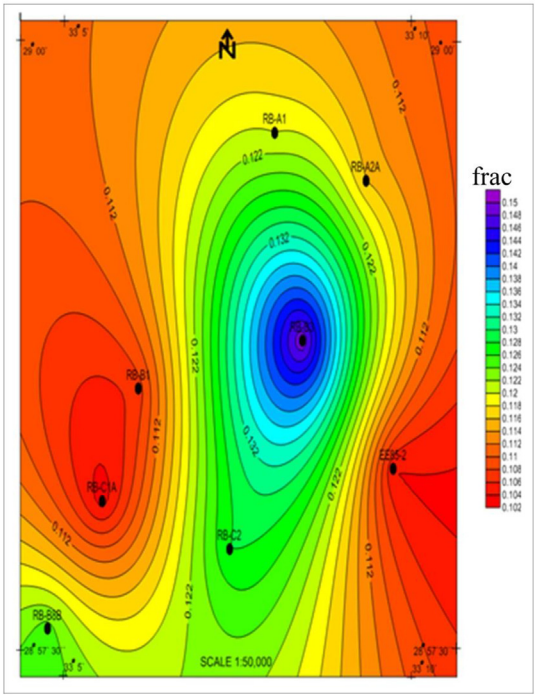

Fig. 7. Dispersed shale distribution map of Raha Formation in the studied area.

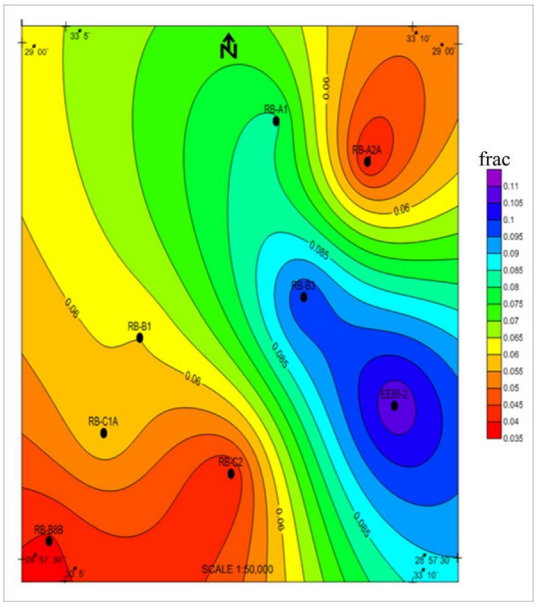

Fig. 8. Laminated shale distribution map of Raha Formation in the studied area.

decrease reaching to 0.035 at RB-A2A well and in the southwest direction reaches 0.037aroun RB-B8B well and gradually increases to the southeastern part of the map where the highest value is recorded 0.108 at EE85-2 well.

4.4.5. Structural shale distribution map of Raha Formation

Fig. 9 exhibits a general low in the southeast direction and the northeast direction while it increases

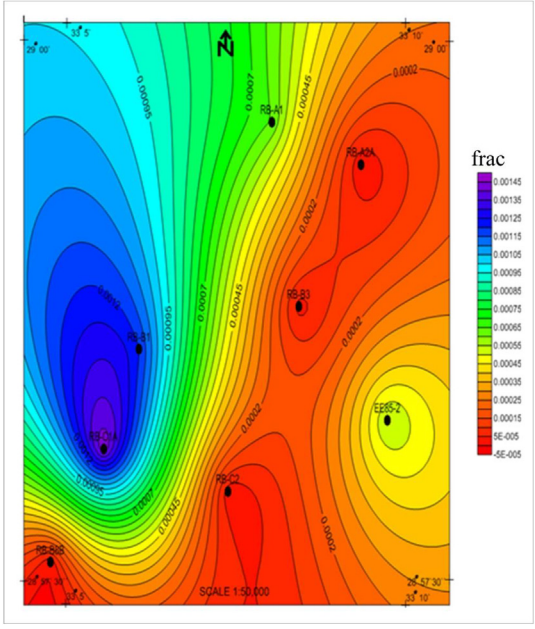

Fig. 9. Structure shale distribution Map of Raha Formation in the studied area.

in the west direction in the study area to give the maximum value (0.00145), which is recorded by RB-C1A well.

4.5. Determination of petrophysical exponents

Water saturation is one of the physical properties of rocks that have links with petrophysical exponents.[20] This relationship may be found in the formation factor (F), where the following equation can be used to express it:

$$F = a/2\varphi m \tag{14}$$

Where:

F: is the formation factor, a: is the tortuosity factor, and m: is the cementation factor.

Sometimes these factors are used as constants, but it is thought that 'a' should be 1 or lower and that the value of 'm' must fall between 1 and 3.

A correlation is observed between formation factors and porosity and permeability.[21] It was demonstrated that the connection with porosity is better and that the formation factor may be represented as follows:

$$F = 1/\varphi m \tag{15}$$

Archie claims that for consolidated sandstones, the cementation factor is almost always between 1.8 and 2.0, and for clean, unconsolidated sands, it is typically around 1.3. Table 1 exhibits the values of 'm' with the comparable reservoir character.

From Table 1, it can be shown that cementing aggregates causes the formation factor values to rise above those seen for aggregates that are not cemented. Furthermore, the cemented aggregates show a larger shift in the formation factor with a change in porosity in comparison to the unconsolidated aggregates.

In addition, as demonstrated by the following equation, the resistivity index depends on the water saturation:

$$I = 1/Swn \tag{16}$$

$$I = Rt/R0 \tag{17}$$

Table 1. The impact of cementation factor on reservoir.

Cementation factor (m)	Rock reservoir character
≃1.3	Unconsolidated rocks
1.4 to 1.5	Very slightly cemented rocks
1.6 to 1.7	Slightly cemented rocks
1.8 to 1.9	Moderately cemented rocks
2 to 2.2	Highly cemented rocks

Where; I is known as the resistivity index while 'n' is known as the saturation exponent (ranges from 1 to 2). While saturation exponent 'n' on consolidated samples from woodbine sand has a value ranging between 2.31 and 2.40.

As previously demonstrated in the Archie and Schlumberger equations for clean and shaly formation water saturation determination, for a more precise estimation of the total water saturation, it is essential to find the accurate values of 'm,' 'n,' and 'a'.[22,23]

Calculating the values of 'm,' 'n,' and 'a' involved using Pickett's plot. The petrophysical parameters were computed using these techniques. For the purpose of evaluating the formation using well-log analysis,[24] the following fundamental connections. As can be seen, the estimation begins with Archie's equation as follows.

$$S_w^2 = \frac{F_R F_w}{Rt} \tag{18}$$

By taking the logarithm with base 10 for this equation,

$$2\log Sw = \log FR + \log Rw - \log Rt \tag{19}$$

By substituting the following equation:

$$FR = a/\varphi m \tag{20}$$

by taking equation (18) we can obtain

$$\text{Log } Rt = \log Rw + \log a - m\log\varphi - 2\log Sw \tag{21}$$

This can be expressed simply as the following form:

$$\text{Log } Rt = -m\log\varphi + \log(aRw) \tag{22}$$

On log-log paper, this equation, which represents a straight line, can be represented as follows:

$$Y = mx + b \tag{23}$$

A straight line with a slope determined by m, where m = 1/slope, can be used to show a plot of log Rt vs. log φ using equation (22).

A distance on the Rt axis is measured, and the slope is calculated by dividing the value by the corresponding distance on the porosity axis.[25] As shown in Fig. 10 for RB-A1 as well as an example, the intersection of such a line with the porosity axis φ = 1 yields the value of aRw. By knowing the value of Rw, the value of tortuosity factor (a) can be determined. According to Pickett,[26] the saturation exponent 'n' which is a function of water saturation equals the value of porosity exponent 'm.' In the Raha Formation via the investigated wells, Table 2 displays the various values for these characteristics.

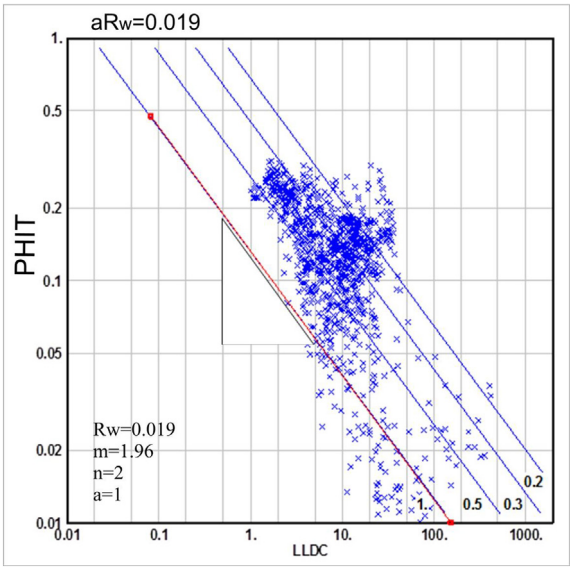

Fig. 10. Pickett's plot of Raha Formation in RB-A1 well in the studied area.

Table 2. The obtained results of the study area.

No.	Well name	Formation	aR_w	a	m
1	RB-AI	RAHA	0.019	1	1.96
2	RB-A2A	RAHA	0.019	1	2.01
3	RB-B1	RAHA	0.014	0.73	2.2
4	RB-B3	RAHA	0.019	1	2.03
5	RB-B8B	RAHA	0.018	0.95	1.97
6	RB-C1A	RAHA	0.019	1	1.78
7	RB-C2	RAHA	0.014	0.72	2.1
8	EE85-2	RAHA	0.018	0.94	2.3

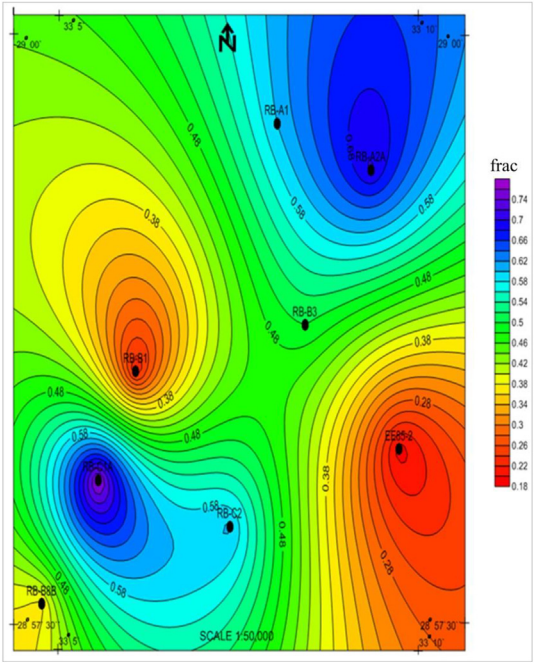

Fig. 11. Water saturation distribution map of Raha Formation in the studied area.

The value of 'm' is ranging between 1.8 and 2.3, while the value of 'a' is varying from 0.70 to 1.0. The saturation exponent 'n' must have a value equal to the value of the cementation factor 'm.' Applying these results to the Archie equation that was used to determine the water saturation in the wells under study, the map (Fig. 11) of Raha Formation demonstrates that the value of water saturation increases toward the northeast and southwest directions around RB-A2A and RB-C1A wells while it exhibits the gradual decrease toward the southeast direction as recorded in EE85-2 well.

4.6. Conclusions

The application of the Dia-Porosity crossplots is very effective and helpful in the determination of the shale types and calculating the volumes of the three shale types. The dominant shale types in the considered formation and area are the dispersed shales. These models are helpful in detecting shale types in the wells in the study area.

In the area under investigation, the total shale volume increases in the center part of the study wells. For the volume of shale types, the dispersed shale shows the highest percentage in the middle of the study area, while the laminated shale volume increases toward the north directions, but the structural shale increases toward the NW direction to give the maximum value. The dominant shale type in the studied area is dispersed shale, which decreases the formation's permeability accordingly. These shale types and their volumes are very important for accurate water saturation.

Also, water saturation determination is began by estimating all the petrophyscial exponents (m, n, and a) which can be determined by using Pickett's plot. These plots depend on the plot of porosity and resistivity on a log-log paper. The resulted plot is shown as a straight line, where from these plots the values of 'm,' 'n,' and 'a' are constructed where their values are very important for the true estimation of water saturation. The value of water saturation increases toward the northeast and southwest directions around RB-A2A and RB-C1A wells while it exhibits a gradual decrease toward the southeast direction, as recorded in EE85-2 well.

Author contributions

Dr.Tarek El Shazly and Dr Ahmed Nooh participated in the writing of the manuscript, and reviewing the draft and final version. Dr. Marwa Elsawy collected the data and was responsible for data analysis, interpretation, preparation, writing,

and submission of the manuscript. Mazen El Bay collected the data, data analysis, and interpretation.

Conflicts of interest

None declared.

References

1. Shazly TF, Ghorab MA, Ghaleb IE, Nabih I. Estimation of the suitable water saturation model of bahariya Formation in sidi barani area, north western desert of Egypt by using well logs analysis. *Int J Acad Res*. 2013;5:35–49.
2. IHS E. *Gulf of Suez Basin Monitor (No. Iris21 ID: 410900*. IHS Energy; 2006.
3. Abdallah AM, Adindani A, Fahmy N. Stratigraphy of the lower mesozoic rocks, western side of the Gulf of Suez. *Rev Geol Survey Mining Res Depart*. 1963;27:23.
4. Elkhadragy AA, Shazly TF, Ramadan M, El-Sawy MZ. Petrophysical investigations to both rudeis and kareem formations, Ras ghara oil field, Gulf of Suez. *Egypt J Petrol*. 2017;29: 269–277.
5. Said R. *Geology of Egypt*. Rotterdam: Balkema; 1990:743.
6. Azab AA, Ramadan MA, El-Sawy MZ. An integrated analysis of gravity and well data for deep-seated structural interpretation: a case study, from Ras Budran oil field, Gulf of Suez, Egypt. *J Pet Explor Prod Technol*. 2019;9:177–189.
7. Naggar AA, Helaly A. *Ras Budrn Field: Geological Aspects and Reservoir Units*. Cairo: 8th EGPC Production Seminar; 1985.
8. Abu Al-Atta M, Issa IG, Ahmed AM, Afife MM. Source rock evaluation and organic geochemistry of Belayim marine oil field, Gulf of Suez, Egypt. 'Review of' accepted: 18 september 2013. *Egypt J Petrol23*. 2014;3.
9. Ghorab MA, Shazly TF, Nooh A, et al. Determining the migration paths through utilization of pore pressure, Belayim Land Oil Field, Gulf of Suez, Egypt: a case study. *Int J Petrochem Natl Gas*. 2022;2:85–97.
10. El-Khadragy AA, Shazly TF, Mousa DA, Ramadan M, El-Sawy MZ. Integration of well log analysis data with geochemical data to evaluate possible source rock, case study from Gm-Alef-1 Well, Ras Ghara Oil Field, Gulf of Suez-Egypt. *Egypt J Petrol*. 2018;27:911–918.
11. Abu El-Ata ASA, Ismail AA. A comparative study between the M-N and Tri-porosity Cross-plots for identifying the matrix components and depositional environments in the central part of the Nile Delta, Egypt. *Ann Geol Surv Egypt*. 1984;1:35.
12. Hilichie DW. *Applied Open Hole Interpretation*. 4. Golden, Colorado: D.W. Hilichie Inc; 1978:88.
13. Abu El- Ata ASA, Shazly TF. A comparative study for detecting the cementation factor, tortousity factor and saturation exponent of Abu Roash Formation in the West Camel Pass Area, Western Desert, Egypt. *Geol Arab World*. 2000;15: 58–83.
14. Atlas Dresser. *Log Interpretation Charts*. 4. Houston, Texas: – Dresser Industries Inc.; 1983:149.
15. Atlas Dresser. Log interpretation charts; Houston. *Dresser Ind*. 1979;2:107.
16. Shazly TF. Geothermal modeling for bahariya Formation of bassel-1x well, northern western desert, Egypt, by using well logs analysis. *J Appl Sci Res*. 2012;8:753–762.
17. Tarek TF, Wafaa AE. Petrophysical evaluation of the upper cretaceous section in ABU Rudeis-Sidri Area, Gulf of Suez, Egypt, using well logging data. *J Appl Geophys*. 2010;7:1–14.
18. Ghorab MA, Shazly TF. Types of shale and their relation with the hydrocarbon fluids of matulla formation in the central part of the Gulf of Suez, Egypt. *J Petrol Mining Eng*. 2004;7:43–69.
19. Schlumberger. Log interpretation. Vol. II. *Appl Paris*. 1974;2: 97.
20. Ghorab MA, Shazly TF, Ghaleb IE, Nabih I. Using of Pickett's plot in shaly formation to estimate the petrophysical exponents of bahariya Formation in sidi barani area, north western desert, Egypt. *Austr J Basic Appl Sci*. 2012;6:399–413.
21. Archie GE. The electrical resistivity logs as an Aid in determining some reservoir characteristics. *Trans AIME*. 1942;146: 54–67.
22. Shazly TF, Ramadan MA. *The Impact of Pickett's Plot for Developing the Petrophysical Model of Abu Roash Reservoir in Ras Qattara Area, Western Desert, Egypt*. Bulletin of the Tethys Geological Society (Bull. T.G.S), Egypt; 2009.
23. Noah AZ, Shazly TF. Integration of well logging analysis with petrophysical laboratory measurements for nukhul formation at Lagia-8 Well, Sinai, Egypt. *Am J Res Commun*. 2014;2: 139–166.
24. Pickett GR. Acoustic character logs and their application in formation valuation. *J Pet Tech Trans, AIME*. 1963;12:639.
25. Ghorab MA, Shazly TF. A comparative study between Pickett's plot and xy cross plot methods on Abu roach formation at the south western of wadi el-natrun area, western desert. *J Appl Sci Res*. 2008;4:1974–1984.
26. Pickett GR. Pattern recognition as a means of formation evaluation. In: *Society of Professional Well Log Analysts 14th Annual Logging Symposium Transactions Paper A*. 1973. A1–A21.